A R C H I V E S O F M E T A L L U R G Y A N D M A T E R I A L S
Volume 53 2008 Issue 1

B. MAJOR* , F. BRUCKERT**, J. M. LACKNER*** , R. EBNER**** , R. KUSTOSZ*****, P. LACKI******

COATINGS ON TiN AND Ti(C,N) BASIS FOR BIOMEDICAL APPLICATION TO BLOOD CONTACT AND TiN/CrN MULTILAYERED TRIBOLOGICAL SYSTEMS PRODUCED BY PULSED LASER DEPOSITION

POWŁOKI NA BAZIE TiN I Ti(C,N) DO KONTAKTU Z KRWIĄ PRZY ZASTOSOWANIU BIOMEDYCZNYM ORAZ TiN/CrN WIELOWARSTWY TRIBOLOGICZNE WYTWARZANE OSADZANIEM LASEREM IMPULSOWYM

Research activity on surface engineering performed at the IMIM PAS in last years has been presented. Experiments were focused on TiN and Ti(C,N) thin coatings produced on titanium and biologically applied polyurethane substrates by application of pulsed laser deposition (PLD), magnetron sputtering (MS), and hybrid PLD/MS, at room temperature. Bio-physical tests of the kinetics of shear flow-induced cell detachment have been carried out. Model eucariotic cells easy to manipulate using technics of molecular biology have been used in experiments. Fluorescence patterns obtained after the performed test at kinetics condition tests have been used to establish kinetics curves. A microstructure examination by application of XRD and transmission electron microscopy have been performed. On the basis of the real cell detachment experiment, a finite element simulation was done. The highest shear stress was estimated for the region of the radius of the whole pierced in the center of the upper disc.

There are an increasing number of applications in tribology where the properties of a single material are not sufficient. One way to surmount this problem is to use a multilayer coating. Application of metallic interlayers improves adhesion of nitride hard layer in multilayer systems. Tribological coatings consisted of 4, 8 and 32 layers of Cr/CrN and Ti/TiN types were fabricated with the PLD technique. It is found in transmission electron examinations on thin foils prepared from cross-section that both nitride-based multilayer structures studied are characterized by small columnar crystallite sizes and high defect density, what might raise their hardness but compromise coating adhesion. The intermediate metallic layers contained larger sized and less defective columnar structure compared to the nitride layers located at close to the substrate which should improve the coatings toughness. Switching from single layer to multi-layer metal/nitride composition improved resistance to delamination.

Keywords: biomedical coatings, microstructure, texture, cell adhesion, tribological multilayers

Przedstawiono działalność IMIM PAN prowadzoną w ostatnich latach w zakresie inżynierii powierzchni. Badania koncentrowały się na cienkich warstwach typu TiN i Ti(C,N) wytwarzanych z wykorzystaniem metody osadzania laserem impulsowym (PLD), magnetronowej (MS) oraz hybrydowej PLD/MS w temperaturze pokojowej na podłożu metalicznego tytanu oraz stosowanego biologicznie poliuretanu. Przeprowadzono testy biofizyczne kinetyki wymywania komórek w warunkach naprężenia ścinania generowanego przepływem. W badaniach zastosowano modelowe komórki eukariota, które są dogodne do wykorzystania w eksperymentalnych technikach biologii molekularnej. Obrazy fluorescencyjne uzyskane po przeprowadzonych testach w warunkach kinetycznych wykorzystane zostały do wyznaczenia krzywych kinetycznych. Przeprowadzono badania mikrostruktury metodą dyfrakcji rentgenowskiej i transmisyjnej mikroskopii elektronowej. Wykorzystując wyniki rzeczywistego eksperymentu wymywania komórek, przeprowadzono modelowanie metodą elementów skończonych. Najwyższe naprężenia ścinające uzyskano dla obszaru leżącego na brzegu otworu centralnego górnego dysku.

Wzrasta ilość zastosowań w tribologii gdy właściwości tworzywa jednowarstwowego są niewystarczające. Jednym z rozwiązań jest wytwarzanie powłok wielowarstwowych. Zastosowanie wielowarstwy metalicznej w układzie Ti/TiN, zawierającym twardą warstwę azotkową, poprawia adhezję. Wytworzone zostały metodą PLD układy tribologiczne składające się z 4, 8 oraz 32 warstw typu Cr/CrN i Ti/TiN. Stwierdzono w badaniach metodą transmisyjnej mikroskopii elektronowej na cienkich foliach uzyskanych z przekroju poprzecznego, że obydwa wielowarstwowe systemy charakteryzują się drobnokrystaliczną strukturą o małej wielkości ziaren kolumnowych z dużą gęstością defektów. Może to wpływać na wzrost twardości, obniżając jednak

* INSTITUTE OF METALLURGY AND MATERIALS SCIENCE, POLISH ACADEMY OF SCIENCES, 30-059 KRAKÓW, 25 REYMONTA STR., POLAND
** LABORATOIRE DES MATERIAUX ET DU GENE PHYSIQUES, TECHN.UNIV.GRENOBLE, FRANCE
*** LASER CENTER LEOBEN, JOANNEUM RESEARCH MBH, LEOBEN, AUSTRIA
**** MATERIALS CENTER LEOBEN, AUSTRIA
***** FOUNDATION OF CARDIAC SURGERY DEVELOPMENT, ZABRZE, POLAND
****** CZĘSTOCHOWA UNIVERSITY OF TECHNOLOGY, 42-200 CZĘSTOCHOWA, 19 ARMII KRAJOWEJ AV., POLAND

adhezję powłoki. Międzywarstwy metaliczne zawierają nieco większych rozmiarów i mniej zdefektowaną strukturę kolumnową niż warstwy azotkowe. Warstwa metaliczna jest pierwszą warstwą przy podłożu i podnosi ona plastyczność powłoki. Przechodząc od warstwy pojedynczej do wielowarstwy typu metal/azotek uzyskuje się poprawę odporności na delaminację.

Introduction

Mono and multi-layer systems for bio-medical and tribological applications, produced by PLD method, have been under complex examination performed at the IMIM PAS in last years. The contribution presents some chosen results of experimental research.

The bulk and surface properties of biomaterials used for medical implants have been shown to directly influence, and in some cases, control the dynamic interactions that take place at the tissue implant interface [1, 2]. These interactions are included in the concept of compatibility, which should be viewed as a bidirectional process between the implanted materials and the host environment that is ongoing through the *in vivo* lifetime of devices. Currently, considerable effort is directed towards the development of engineered surfaces that could elicit rapid and highly precise reactions with cells and proteins, tailored to specific applications. Titanium nitride (TiN) is expected as a perspective biomaterial, however, it is currently observed that carbide and carbonitrides Ti(C,N) coatings become popular [2]. Before they being applied it has to be evaluated and meet particular requirements depending on the proposed location in the body.

The present work is focused on microstructure, texture and mechanical diagnosis which consider nitrogen and carbon influence on adhesion and structure behavior of coatings. Surface of material strongly influences on the stress formation in the case of biological tissue by the flow of the liquid medium, thus shear stress formation was of detail studied. Cell detachment assay has been applied to verify the coating influence on stress system formation between the surface of the biomaterial and biological cell.

Reaching of improved stability mechanical demands and reducing the use of hazardous lubricants are the basis for search of new tribological systems [3-7]. High hardness and temperature strength, chemical and high toughness are demanded by coatings. In order to reduce friction and wear, the tool surface has to form stable compounds at the contact interface. As generally recognized, it is impossible to combine all these properties together in a single conventional tool material. Leading to tailor-made composite and surface-engineered materials, a large variety of functional properties can be optimized separately for bulk material and surface by applying appropriate coatings. Titanium nitride coatings, have been widely accepted in a range of industrial applications with high demands on wear resistance and adhesion to the substrate. They could be deposited using different techniques and are still one of the most popular hard coatings in industry [3-11]. However, requirements to withstand aggressive environments at elevated temperatures have resulted in switching interest to chromium nitride coatings, which form a surface passive oxide layer stopping their further degradation [5-7].

The presented research work is focused on fabrication and examination of tribological nanocrystalline Cr/CrN and TiN/CrN multilayers. Systems comprising 2, 4, 8, 32 and 64 layers with total thickness 1 μm produced by the PLD technique at room temperature is under examinations.

Experimental

1. Biomedical coatings on TiN and Ti(C,N) basis

1.1. Deposition

For deposition, the PLD method (pulsed laser deposition) was applied [3,8-11]. Before deposition of the main coating, a buffer film was applied. The layout of the proposed coating design is presented in Fig. 1. It was deposited with the changing of gas flow conditions. The main deposition parameters are presented in Table 1. There is a strong influence of the atmosphere on the plasma plum shape. For vacuum 2×10^{-3} Pa the evaporated particles like, ions and atoms cloud, has a spheritic shape. High kinetic energy is expected under such conditions, which could have an influence on thickness inhomogenity. Reactive gas flow introduction into the reactive chamber causes visible change of the plasma shape, thus lowering energy of the particles but increasing uniformity of the material distribution on the substrate. Nowadays, carbide and carbonitride coatings seem to be more popular for medical application, thus three different series of materials were taken under investigation: i.e. stoichiometric TiN, Ti(C,N) deposited under 0.5 cm^3/min acetylene flow, and Ti(C,N) deposited under the 5 cm^3/min acetylene flow. Coatings were fabricated onto pure titanium substrate.

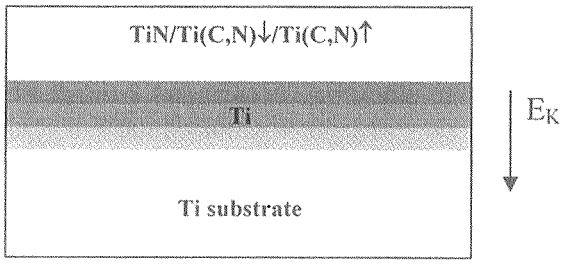

Fig. 1. The layout of the coating material equipped with buffer layer

TABLE 1
Deposition parameters of coatings with the applied buffer layer

Sample	Symbol	Coating	Deposition time/Gas flow during buffor layer deposition	Gas flow during main coating deposition
1	TiN	500nm TiN	4' 0sccm Ar 4' 10 sccm Ar 5' 30 sccm Ar	60' 30sccm N_2
2	Ti(C,N)-3	500nm Ti(C,N)	4' 0sccm Ar 4' 10 sccm Ar 5' 30 sccm Ar	60' 29.5sccm N_2 + 0.5sccm C_2H_2
3	Ti(C,N)-5	500nm Ti(C,N)	4' 0sccm Ar 4' 10 sccm Ar 5' 30 sccm Ar	60' 25sccm N_2 + 5sccm C_2H_2

* sccm- standard cubic cm per minute (cm^3/min)

1.2. TEM examinations

Starting (buffer) layer was elaborated to produce a bridge between the substrate and the coating. Some of the reflections of the buffer layer have the similar lattice spaces to the main coating TiN. (Fig. 2). As it was proved by electron diffraction, the buffer layer was composed of titanium oxide. Thus, interactions between titanium oxide and titanium nitride were investigated. The similar positions of the following reflexes from the buffer layer: (021TiO_2), (202TiO_2), (311TiO_2) (220TiO) and (200TiN), (220TiN), (311TiN) and (101Ti_2N) of the main TiN coating proves orientation transformation. Indexing was carried out using Labar program [12]. Kinetic conditions in the reactive chamber could strongly influence the crystallization degree. High resolution transmission electron microscopy was used to analyze microstructure of the thin buffer film (Fig. 3a). It was verified in use of Fourier transform (Fig. 3b). Rings characteristic for amorphous structure for the applied vacuum deposition conditions were stated. For the maximal neutral gas flow, the diffraction presents images characteristic for a crystallized material. A crystallization degree highly depends on the neutral gas flow in the reactive chamber which influences the kinetic energy of the particles. High resolution transmission electron microscopy technique was used to analyze the main coating microstructure.

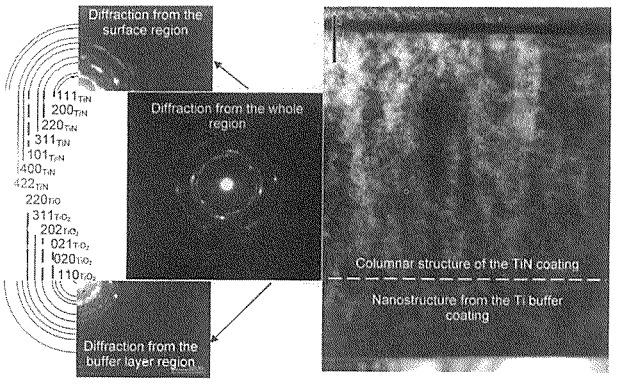

Fig. 2. Orientation transformation from the buffer layer to the main coating TiN; diffractions were calculated by [6]

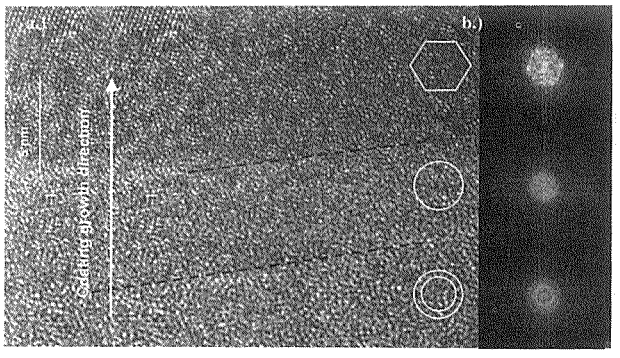

Fig. 3. a) HRTEM microstructure of the buffer coating b) Fourier transform

1.3. X-Ray texture tomography (XTT)

The influence of the reactive gas flow in the reactive chamber on the type of texture was analysed in use of the x-ray diffraction technique. Texture tomography (XTT) is noninvasive technique for the crystallographic orientation measurement [13]. It allows to establish crystallographic texture at the constant deepness of the X-ray penetration. The strongest axial character was found for the stoichiometric TiN (Fig. 4a). For the Ti(C,N) disturbances were observed (Fig. 4b). With the increase of acetylene flow (10 times), the come back to the axial orientation was observed. (Fig. 4c). The most dominant component for the TiN was (110) with intensity about 8. Next (223) with the 0.8 intensity. No (111) reflexes were detected. In the case of Ti(C,N) deposited with the low acetylene flow (0.5 cm^3/min), (111) component was detected with 1.6 intensity. The strongest orientation was (102) with intensity 1.4, then (123) with 0.8 intensity. No (223) reflexes were detected. The second serie

of Ti(C,N) coatings, deposited under a higher acetylene flow was characterized by (102) as the most dominant component with 2.2 intensity and the next components as follows (111)- intensity 2.0, (123)- intensity 0.7. The intensity from (223) plane was very low.

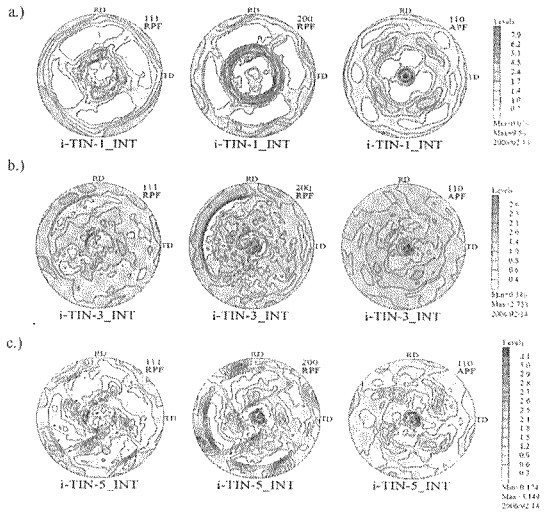

Fig. 4. Pole figures of crystallographic texture a) TiN b) TiCN 0.5 sccm C_2H_2 c) TiCN 5 sccm C_2H_2

1.4. Tribological investigations – Scratch test

Rockwell C method was used for investigations. Results are presented in Table 2. The first cracks for TiN coatings appeared for 3N load. Cracks were of "buckling" type. The substrate was uncovered for 9 N load. For Ti(C,N)-3, the first cracks appeared for 3.4 N. The cracks were of "buckling" type. Simultaneously with friction coefficient increase, the substrate uncover was observed for 9 N load. For Ti(C,N)-5 sample, the first cracks appeared for 1.6 N but there were small cohesive type cracks. "Buckling" cracks appeared for 3.5 N of the applied load. This coating was more brittle comparing to the others.

TABLE 2

Scratch test results

Sample	Pmax [N]	L_c [N]	h [μm]	The load of the wear visible		h_{max} [μm]	h_{rez} [μm]
				Buckling type cracks	Substrate uncover		
TiN	10	2.9	4.5	2.9	9.5	12.8	5.3
				Buckling type cracks	Sunstrate uncover		
Ti(C,N)-3		3.4	5.8	3.4	8.6	15	5.7
				Cohesive cracks	Buckling type cracks		
Ti(C,N)-5		1.6	3	1.6	3.6	14	6

1.5. BIO kinetics – Cell detachment

A *Dictyostelium discoideum* was used as a model organism to study cell detachment kinetics [14]. In the case of *D. discoideum* a unicellular eukaryote also able to complete a pluricellular development cycle, membrane adhesiveness is tightly related to lifestyle. In the vegetative phase, the small (8-μm diameter) ameba feeds upon bacteria and yeast by phagocytosis. Plasma membrane adhesion is therefore directly related to the phagocytic properties of the cell. In the development phase, cell-cell adhesion is more important, and specific contact proteins are expressed [15]. Axenic strains showing an enhanced fluid-phase endocytosis have been obtained and are able to grow in suspension in nutritive medium [16]. The sequencing of *D. discoideum* 34-Mbp genome and Expressed Sequenced Tags from various developmental stages are currently in a completion phase [17]. The available molecular tools make *D. discoideum* was a good model organism to study phagocytosis and cellular motility using null or overexpression mutants [15, 16]. Several mutant studies suggested the existence of three kinds of adhesion protein. A glucose-selective lectin, mediating attachment of bacteria to the cell, was revealed by the sensitivity of mutants to 50 mM glucose. A hydrophilic receptor called Phg1, consisting of a 9-helix transmembrane protein was recently identified. As for now, the molecular nature of its ligand is unknown, but it is present in nutritive media, because Phg1 null mutants are adhesion defective in this medium. The third class of the adhesion molecule is sensitive to surface hydrophobicity, as exemplified by the HV32 mutant, which does not bind to polystyrene in the presence of glucose. For a given cell, detachment occurs for values of the applied hydrodynamic pressure above the threshold. In this purpose, a radial flow detachment essay was used. Cells were re-suspended in the Sörensen buffer and spread at a density of 300 cells /mm^2 on the substrate surface and subsequently submitted to the shear flow under the radial geometry. The temperature of the liquid was kept constant at 21°C. A radial hydrodynamic flow was generated between the stainless disc and sample on which cells adhered. The stainless steel disk with a hole in the center was placed above the sample with the 100 μm distance. The action of the shear flow depends on the distance between the disc and the sample and the level of the upper tank influence on the shear stress between the cells and the material surface. The layout of the investigation is presented on Fig. 5.

After the test, samples were given under the fluorescence microscopy observation. In use of Image-ProPlus software, the cells were counted and on basis of the received values critical shear stress was calculated in use of the following formula (1):

$$\sigma_{50\%} = \frac{3D\eta}{\pi r_{50\%} e^2} \quad (1)$$

$r_{50\%}$ is the distance to the center where 50% of cells are detached D – rate during the test, η – buffer viscosity.

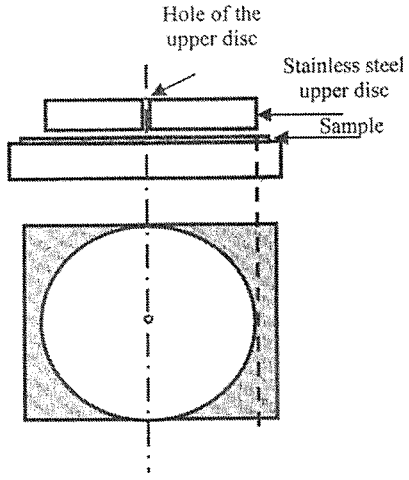

Fig. 5. Cell detachment assay equipment layout

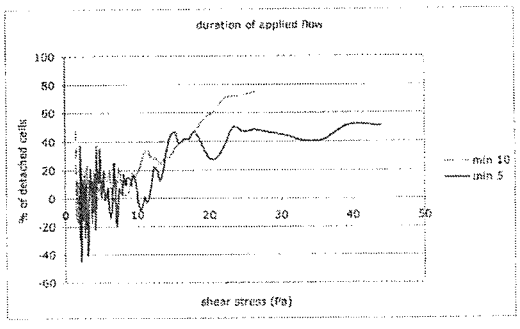

Fig. 6. Cell detachment kinetics for titanium substrate in two exposition times

In order to receive stagnation point, the considered time of the test changed from 5 to 10 minutes. Fig. 6 presents hydrodynamic stress as a function of detached cells for titanium substrate in 5 and 10 minutes of the test durable. The test time increase caused that more cells detached. It was observed that shear stress should be applied for longer times to determine detachment kinetics. Titanium nitride coating was expose for the three deferent test durable, 5, 10 minutes. The longer the time is the more cells are detached. Comparing the results between the substrate and the coating, 20% more cells remained on the uncoated substrate (Fig. 7). In conclusion to this result shear stress should be applied for longer times to determine detachment kinetics. Fig. 8 presents detachment kinetics for titanium carbonitride with low carbon content. It was observed no clear difference between 5 and 10 min, thus steady state is almost reached.

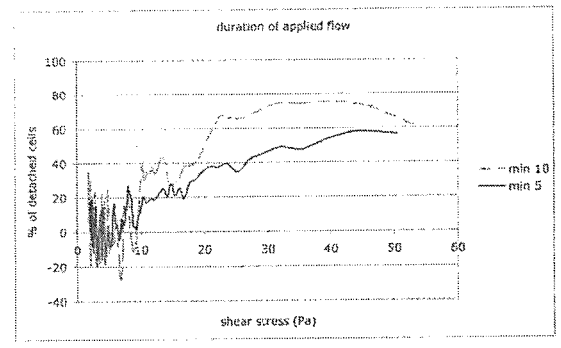

Fig. 7. Cell detachment kinetics for titanium nitride coating in two exposition times

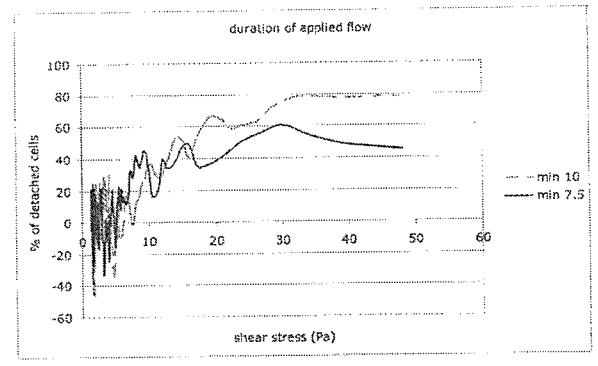

Fig. 8. Cell detachment kinetics for titanium carbonitride with low carbon content coating in two exposition times

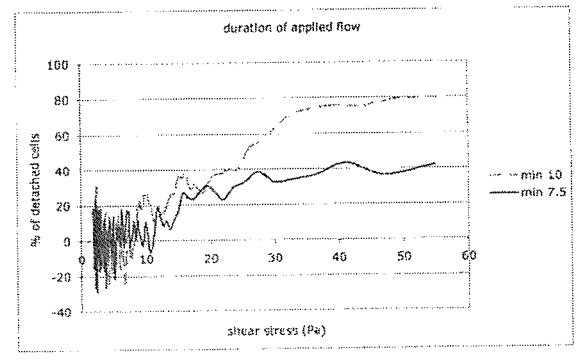

Fig. 9. Cell detachment kinetics for titanium carbonitride with high carbon content coating in two exposition times

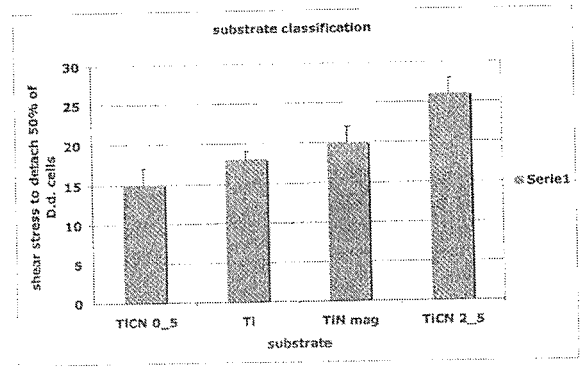

Fig. 10. Shear stress classification

The results associated with titanium carbonitride with high carbon content are presented in Fig. 9. Shear stress should be applied for longer times to determine detachment kinetics.

In summary, the total values of the shear stress was collected and compared. Fig.10 presents total classification of the shear stress which was detected between the coating and the biological cell. The percentage of detached cells was recalculated as a function of shear stress, since not so many cells were detached, the initial density from the distribution of remaining cells was taken. The center of the distribution was always between 190 and 205 frames. The value that makes the distribution symmetrical was put. Sometimes, the distribution was not symmetrical. The center and the percentage of detached cells was shown as a function of shear stress. Data obtained for 10 min flow to data obtained after shorter flow duration were compared. In the Fig. 10 there are shear stress ordered as a function of material: The less adhesive one is TiCN 0_5, the order is TiCN 0_5 < Ti = TiN magnetron < TiCN 2_5. Stress values are presented in Table 3.

TABLE 3

Shear stress values for the selected materials

	Critical shear stress $\sigma_{50\%}$ [Pa]
Ti substrate	18
TiN coating	20
Ti(C,N) (C ↓)	15
Ti(C,N) (C ↑)	26

1.6. Finite element modeling

On the basis of the real cell detachment experiment, a finite element simulation was done. The real material properties were considered for titanium nitride. A medium viscosity was introduced for the calculations as well. The highest shear stress was estimated for the region of the radius of the whole pierced in the center of the upper disc (Fig. 11). Shear stress distribution presented in the FEM illustration relatively is similar to the results obtained experimentally.

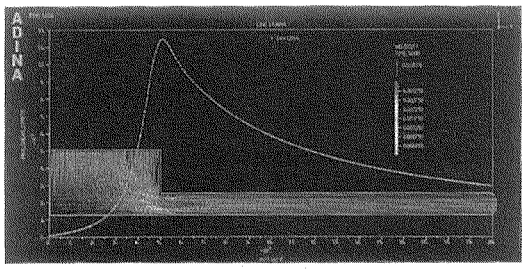

Fig. 11. Finite element modeling of the cell detachment experiment

1.7. Final remarks

Hybryd PLD method has a lot of possibilities for the surface design modifications. There was new coating design proposed in the work.

- Buffer layer was deposited under the main coating to produce bridge for the substrate orientation generation to the main TiN coating. The buffer layer was deposited under the increasing kinetic energy conditions by the gas flow change.
- Parameter optimization like deposition time, reactive gas flow, geometry of the laser optics, allows to achieve biocompatybile coatings with nanocrystalline structure. The gas flow varied between vacuum and 30 sccm (cm^3/min). It has an influence on kinetic energy of the particles and plasma plum flow. It concerns the structure modification from amorphous to crystallized.
- Biocompatibility was regarded in aspect of biophysics and the cell kinetic adhesion description. There were found differences of the shear stress values and the percentage of the detached cells between the titanium substrate surface and the surface of the coating.

2. Multilayer tribological systems

2.1. Materials and methods of examinations

Multilayer coatings based on Cr/CrN and TiN/CrN systems were deposited onto austenitic and ferritic steels. High purity targets (99.9%Ti and 99.9%Cr) were used in ablation experiments with a pulsed Nd:YAG laser system operating at 1064 nm wavelength with 0.6 J pulse energy and 10 ns pulse duration at a repetition rate of 50 Hz. Targets were rotated during the laser irradiation in order to avoid the formation of deep craters. The emitted species were deposited at room temperature (approx. 25°C) onto substrates mounted parallel to the target surface at total pressure: from vacuum (10^{-5} mbar) to 4 Pa and continuous flow of N_2 (99.999%) of order of 30 sccm. To provide homogenous film thickness over the whole coated surface, the substrates were moved through the plasma plumes during deposition. No bias was used.

2.2. Coating design

The fabricated coatings consisted of 2, 4, 8, 32 and 64 Cr/CrN and TiN/CrN layers, respectively, with the total thickness of 1 μm. They were deposited using the same procedure, i.e. the titanium or chromium target ablation was started under low argon pressure atmosphere and subsequently at intervals corresponding to the de-

signed nitride layers, nitrogen mixed with argon was introduced.

2.3. Thin foils preparation and TEM observation conditions

Transmission electron microscopy (TEM) analysis was performed on a Tecnai G^2F20 (200kV) and JEOL EX4000 (400 kV). Microstructure investigations were carried out on the cross-section of coatings. An Energy Dispersive Spectroscopy (EDS) Phoenix EDAX analyzer was used for local chemical analysis. Focus Ion Beam (FIB) or "tripod" polishing followed by an Ar^+ ion milling has been applied for thin foils preparation.

2.4. Mechanical testing

Microhardness was analyzed by the Vickers method. Adhesion was examined by a scratch test (Rockwell HRC penetrator). The applied scratch length was 2 mm on which load increased linearly from 0.03 N up to 30 N.

2.5. Cr/CrN multilayer coatings

2.5.1. Microstructure analysis

Four layered coating of Cr/CrN composition was produced using single Cr target. Multilayer composition was obtained by switching in between non reactive (Ar) and reactive (N_2) gas flow through the deposition chamber. Cr layer was deposited as a first buffer layer on the substrate to increase adhesion of the coating to the substrate. Phase analysis has been confirmed by selected area diffraction patterns (Fig. 12).

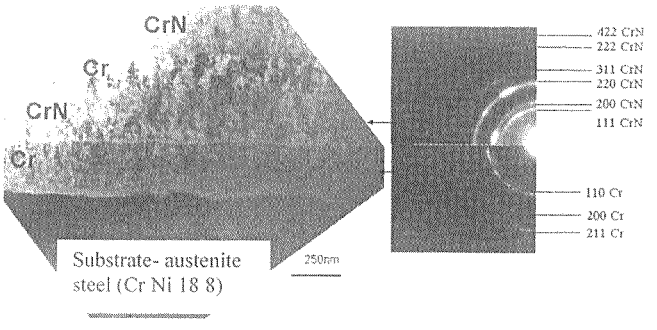

Fig. 12. TEM microstructure and electron diffractions of the cross-section of the 4 – layered Cr/CrN coating

A columnar character in nanocrystalline grains was stated in each case (Fig. 13). Microstructure of layers in the presented coatings was strongly defected due to the deposition conditions applied. In all coatings, the first pure chromium buffer layer was built of much smaller crystallites than intermediate ones. Strong diffraction contrast of the interface could be originated from the lattice distortion in the neighborhood of misfit dislocations. The high resolution electron microscopy technique (HRTEM) confirmed the columnar character of Cr grains and their dominant orientation as well as exhibited much smaller CrN grains. Very small CrN grains overlapped what caused formation of the Moire fringes in the image (Fig. 14).

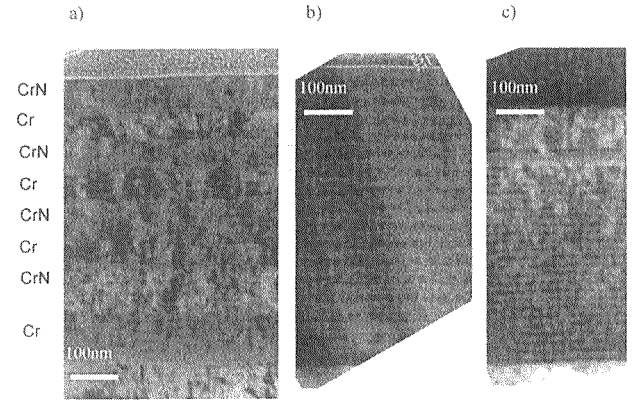

Fig. 13. TEM microstructure of the cross-section of: a) 8 – layered; b) 32 – layered; c) 64 – layered Cr/CrN coating

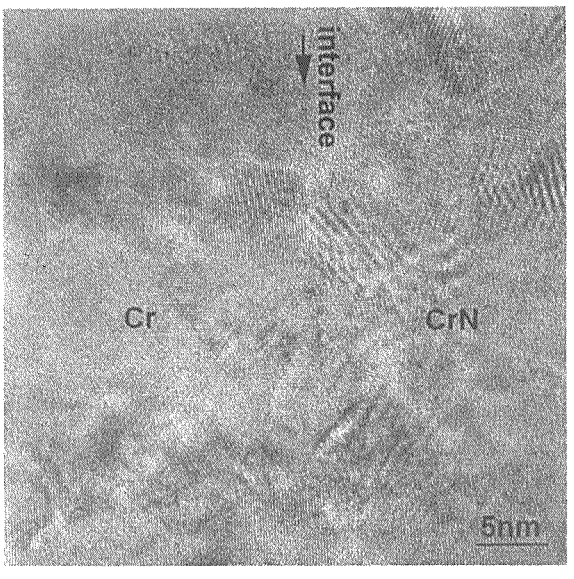

Fig. 14. HRTEM microstructure of the Cr/CrN interface in the 8 – layered coating

2.5.2. Tribological properties

Microhardness was measured using the Vickers indenter for the 20 mN of the applied load and results are presented in Fig. 15. The highest value of microhardness among the examined multilayer coatings was detected for

the 8-layered system. Coatings containing higher amount of layers exhibit decrease of properties with increasing number of layers. Adhesion was analyzed by the scratch – test. In the case of the single Cr layer, the first cracks appeared under the load of 21 N. Cracks were observed along the scratch path border. This type of cracks could

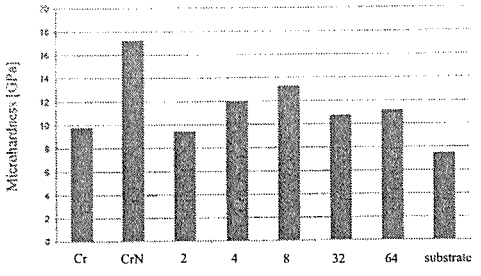

Fig. 15. Microhardness results of Cr/CrN multilayer coatings for 20 mN of the applied load of the indenter; pillars from left to right: Cr, CrN, Cr/CrN2, Cr/CrN4, Cr/CrN8, Cr/CrN32, Cr/CrN64, substrate

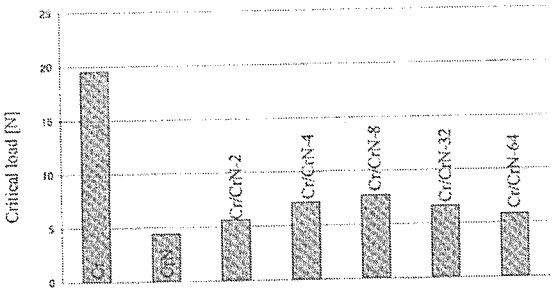

Fig. 16. Scratch- test results of Cr/CrN multilayer coatings

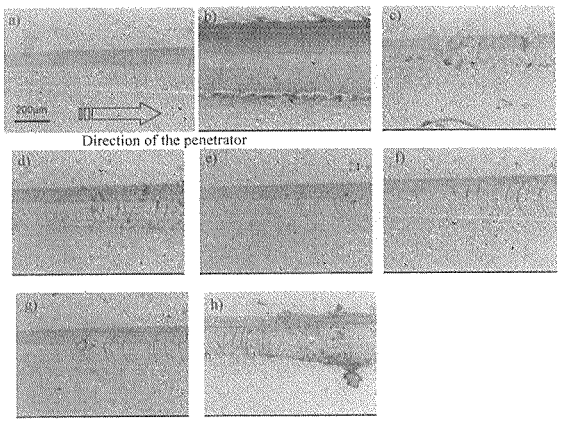

Fig. 17. Images of the scratch tracks of: a) Cr under 5 N of the applied load of the indenter; b) Cr under 30 N of the applied load of the indenter; c) CrN; d) Cr/CrN 2-layered; e) Cr/CrN 4-layered; f) Cr/CrN 8-layered; g) Cr/CrN 32-layered; h) Cr/CrN 64-layered

be effected by the plastic deformation of the coating under the relatively high load of the indenter. Such type of wear could inform about a strong adhesion of coating to substrate. CrN single layer was brittle, the first cracks appeared under 4 N of the applied load. Multilayer Cr/CrN coatings showed unconformal type of buckling cracks. They were characterized by intermediate value of the applied load in comparison with single Cr and CrN layers. Their critical load was in the range of 6-8 N. Results are presented in the diagram (Fig. 16) and their character has been presented in images (Fig. 17). The highest critical load among multilayer coatings was established for the 8-layered coating. The range for the highest critical load is in a good agreement with those of the highest microhardness.

2.6. TiN/CrN multilayer coatings

2.6.1. Microstructure analysis

TiN/CrN coatings were produced using two types of Ti and Cr targets. TiN layer was deposited at the constant flow of nitrogen through the chamber as the first one to enhance the adhesion of the total coating to the substrate. Phase analysis was confirmed by selected area diffraction pattern (Fig. 18). Both layers are built of columnar crystallites. TiN grains are finer than CrN. The average dimension of them is ~25nm, while CrN is ~40nm. In the case of the TiN layer, spots observed on diffraction rings were more blurred and extended than CrN ones. Coatings built of higher number of layers with the same total thickness of coating were characterized by the similar microstructure to the 2-layered coating. The microstructure was strongly defected. With increasing number of layers, crystallites were smaller and more coarsened. In each case of analyzed coating (2, 8 and 32-laers) the first TiN buffer layer was built of much smaller crystallites than intermediate ones (Fig. 19).

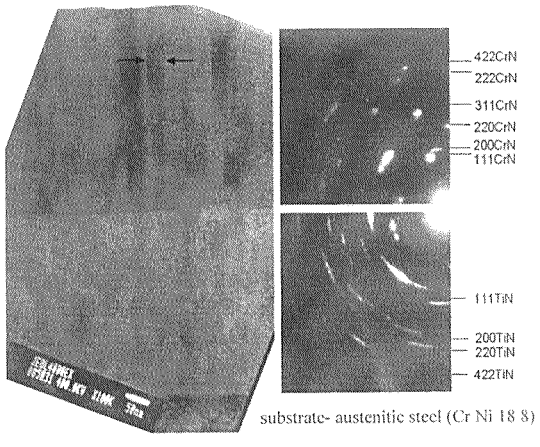

Fig. 18. TEM microstructure and electron diffractions of the cross-section of the 2-layered TiN/CrN coating

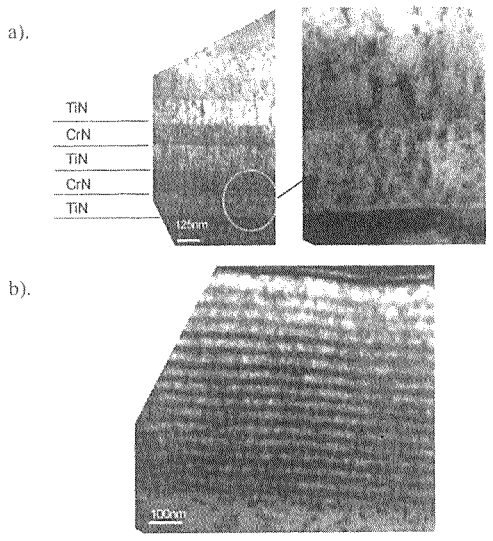

Fig. 19. TEM microstructure of the cross-section of: a) 8-layered TiN/CrN coating; b) 32-layered TiN/CrN coating

2.6.2. Tribological properties

Results of microhardness analysis for the 20 mN applied load of the Vickers indenter are presented in the diagram (Fig. 20). The obtained results for TiN/CrN system confirmed behavior assessed for Cr/CrN multilayer coatings. The 8-layered coating had the highest value of microhardness while 32-layered coating presented decrease of hardness. Adhesion was analyzed by the scratch-test. In this group of multilayer coatings, cracks which appeared under the indenter had the conformal character. The critical load for them was established in the range of 6-8 N. Results are presented in the diagram (Fig. 21) and their character has been presented in images (Fig. 22). The highest critical load was noted for the 8-layered coating. This result was in a good agreement with that one which was obtained in the case of microhardness measurements of this type of coatings as well as with results obtained for the Cr/CrN system.

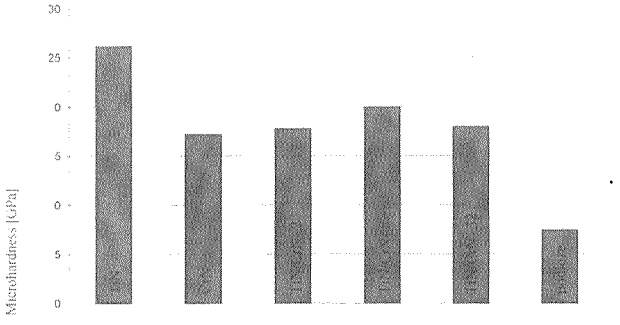

Fig. 20. Microhardness results of TiN/CrN multilayer coatings for 20 mN of the applied load of the indenter; pillars from left to right: TiN, CrN, TiN/CrN2, TiN/CrN8, TiN/CrN32, substrate

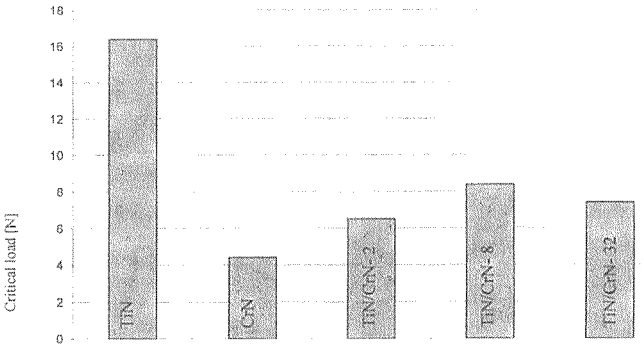

Fig. 21. Scratch- test results of TiN/CrN multilayer coatings

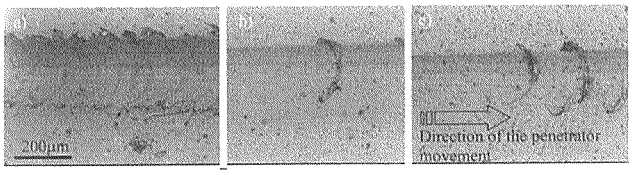

Fig. 22. Images of the scratch tracks of: a) TiN/CrN 2-layered; b) TiN/CrN 8-layered; c) TiN/CrN 32-layered

2.7. Discusion

Both types of Cr/CrN as well as TiN/CrN coatings were characterized by the ultra-fine character of crystallites in the first buffer layer. Intermediate layers contained much bigger, columnar grains which diameter was in the range of 10-30 nm. HRTEM observations of the Cr/CrN interface pointed out at some relations of orientations in-between individual layers in the multilayer composition. Interfaces in multilayer composition as well as surface of coatings are of crucial points. There are only some very small waviness noticed in the range of 2 nm in the 1 µm length of analyzed area. The goal of experiments was to maximize the number of layers with the constant total thickness of coating which was 1 µm. In the case of the 64-layered coatings, the thickness of individual layer was approximately 15 nm. Results of observation of multilayer coatings shown a jumping transfer between consisting layers in an atomic scale thus the PLD method could be used to deposit layers with modulation approaching 10 nm. The observed maximum of hardness in Cr/CrN coatings in relation to a number of layers indicated an effect of coating hardening up to a moment of crystallite transformation to a nanocrystalline range. Such an effect is observed just at about thickness of constituting layer of about 125 nm. Results of the work confirmed that optimization of relation between the ceramic and metallic layer could lead to fabrication of multilayer systems with improved mechanical properties.

3. Conclusions

- Deposited Cr/CrN and TiN/CrN coatings comprised equiaxual crystallites in the range of 1 to 10 nm in the part contacting with the substrate i.e. buffer layer.
- Buffer layers in each case were built from much smaller crystallites than intermediate ones.
- Fine grained defected columnar microstructure was observed in the intermediate and surface part of coatings.
- Microstructure revealed in coatings was strongly defected due to deposition process.
- Analysis of mechanical properties indicated that 8 layer coating has optimal mechanical properties for both examined type of systems.

Acknowledgements

The work was supported by the PBZ-KBN-100/T08/2003 project from the means provided by the Polish Ministry of Science and Higher Education as well as by the FP6 Knowledge-based Multicomponent Materials for Durable and Safe Performance KMM NoE project. Financial support by the Austrian Federal Ministry of Traffic, Innovation and Technology, the Government of Styria and the European Union is highly acknowledged.

REFERENCES

[1] J. A. Helsen, H. J. Breme, Metals as Biomaterials, Wiley, Baffins Lane, Chichester, West Sussex, England 1998.

[2] B. D. Ratner, A. S. Hoffman, F. J. Schoen, J. E. Lemons, Biomaterials Science, Elsevier Inc. 1 (2004).

[3] D. S. Rickerby, A. Matthews, eds., Advanced Surface Coatings: a Handbook of Surface Engineering, Chapman and Hall, New York 1991.

[4] J. E. Greene, Physics of film growth from the vapor phase, in Multicomponent and Multilayered Thin Films for Advanced Microtechnologies: Techniques, Fundamentals and Devices, edited by Auciello O., Engemann J., Kluwer Academic Publishers, NATO ASI Series E: Applied Sciences **39**, 234 (1993).

[5] S. J. Bull, D. S. Rickerby, Compositional, microstructural and morphological effects on the mechanical and tribological properties of chromium nitrogen films, Surf.Coat.Technol. **43/44**, 732 (1990).

[6] Y.L. Su, S. H. Yao, Z. L. Leu, C. S. Wei, C. T. Wu, Comparison of tribological behaviour of three films – TiN, TiCN and CrN- grown by physical vapour deposition, Wear **213**, 165 (1997).

[7] S. A. Barnett, A. Madan, I. Kim, K. Martin, Stability of nanometer- thick layers in hard coatings, E-MRS Bulletin **28**, 169 (2003).

[8] D. B. Chrisey, G. K. Hubler, (Eds.), Pulsed Laser Deposition, John Wiley, New York 1994.

[9] J. C. Miller, R. F. Jr Haglund, (Eds.), Laser Ablation and Desorption, Academic Press, San Diego 30 (1998).

[10] D. Bäuerle, Laser Processing and Chemistry, Springer-Verlag, Berlin, Heidelberg 2000.

[11] J. M. Lackner, Industrially-scaled hybrid Pulsed Laser Deposition at Room Temperature: Published by Orekop sc., Kraków, Poland 2005.

[12] J. L. Lábár, Consistent indexing of a (set of) SAED pattern(s) with the ProcessDiffraction program; Ultramicroscopy **103**, 237 (2005).

[13] J. T. Bonarski, X-ray texture tomography of near surface areas, Progress in Materials Science, 2006, 51, 61-149; (Polish version) Rentgenowska Tomografia Teksturowa: Copyright by Instytut Metalurgii i Inżynierii Materiałowej PAN, Kraków 2001.

[14] S. Bozzaro, E. Ponte, Cell adhesion in the life cycle of Dictyostelium, Experientia **51**, 1175 (1995).

[15] J. M. Ashworth, D. J. Watts, Metabolism of the cellular slime mould Dictyostelium discoideum grown in axenic culture. Biochem. J. 119, 175 (1970).

[16] T. Morio, H. Urushihara, T. Saito, Y. Ugawa, H. Mizuno, M. Yoshida, R. Yoshino, B. N. Mitra, M. Pi, T. Sato, K. Takemoto, H. Yasukawa, J. Williams, M. Maeda, I. Takeuchi, H. Ochiai, Y. Tanaka, The Dictyostelium discoideum developmental cDNA project: generation and analysis of expressed sequence tags from the first-finger stage of development. DNA Res. 5, 335 (1998).

[17] F. Bruckert, M. Demily, Y. Brecht, L. Boulangé, Kinetics of yeast detachment from controlled stainless steel surfaces; Colloids and Surfaces B, Biointerfaces, Elsevier Inc. **51**, 71 (2006).

Received: 3 December 2007.